ADVANCED MATERIALS
www.advmat.de

Thickness of Nanoscale Poly(Dimethylsiloxane) Layers Determines the Motion of Sliding Water Drops

*Xiaoteng Zhou, Yongkang Wang, Xiaomei Li, Pranav Sudersan, Katrin Amann-Winkel, Kaloian Koynov, Yuki Nagata, Rüdiger Berger, and Hans-Jürgen Butt**

Layers of nanometer thick polydimethylsiloxane (PDMS) are applied as hydrophobic coatings because of their environmentally friendly and chemically inert properties. In applications such as heat exchangers or fog harvesting, low water drop friction on surfaces is required. While the onset of motion (static friction) has been studied, the knowledge of dynamic friction needs to be improved. To minimize drop friction, it is essential to understand which processes lead to energy dissipation and cause dynamic friction? Here, the dynamic friction of drops on PDMS brushes of different thicknesses is measured, covering the whole available velocity regime. The brush thickness *L* turns out to be a predictor for drop friction. 4–5 nm thick PDMS brush shows the lowest dynamic friction. A certain minimal thickness is necessary to form homogeneous surfaces and reduce the attractive van der Waals interaction between water and the substrate. The increase in dynamic friction above $L = 5$ nm is also attributed to the increasing viscoelastic dissipation of the capillary ridge formed at the contact line. The height of the ridge is related to the brush thickness. Fluorescence correlation spectroscopy and atomic force measurements support this interpretation. Sum-frequency generation further indicates a maximum order at the PDMS–water interface at intermediate thickness.

1. Introduction

Environmentally friendly polydimethylsiloxane (PDMS) coatings are often used to fabricate hydrophobic surfaces.[1] These surfaces can help to reduce interfacial friction,[2] and exhibit antifouling and anti-icing properties.[3] One way to coat PDMS is by chemically anchoring PDMS chains to substrates,[4] which prevents surface depletion.[5] In this case, one end of the polymer chain is fixed on the substrates by the covalent bond, the rest of the chain is free to rotate, bend, and stretch due to the low glass transition temperature (<−100 °C) of PDMS.[6] Such surfaces are called covalently attached liquid surfaces (CALS)[1] or an omniphobic liquid-like surface.[6] Limited by the length of the polymer chain and its tendency to pack randomly, the film thickness of CALS is typically a few nanometers.

When a liquid drop is placed on a soft layer, the surface tension of the liquid exerts a tensional force at the contact line.[7] As a result, the layer shape is locally changed and capillary ridges are formed. In contrast to micrometer thick PDMS layers, deformation at the contact line on polymer brushes is only of the order of the brush thickness, as shown by computer simulations.[8] It is too small to be resolved by optical methods.[7a,9] or even X-rays.[10] Less energy is dissipated on a nanoscopic layer than on thick PDMS layers.[11] This liquid-like behavior in combination with low viscoelastic energy dissipation in thin layers makes PDMS CALS a promising coating for use in applications such as fluid manipulation, in heat exchangers, and in microfluidic applications.[12] In engineering applications, it is important that drops move fast, with little resistance.[13] Here, we study the dynamic drop friction of water drops on PDMS CALS. The aim is to identify conditions minimizing drop friction.

The friction force F acting on the onset of drop is typically measured by placing a water drop on a solid surface and then tilting the surface until the drop starts sliding off at a tilt angle α. Low roll-off angles α indicate low static friction.[14] The reason for such low roll-off angles is low contact angle hysteresis. Drops slide off surfaces once the gravitational force, $mg\sin\alpha$ (m is the drop mass,

X. Zhou, Y. Wang, X. Li, P. Sudersan, K. Amann-Winkel, K. Koynov, Y. Nagata, R. Berger, H.-J. Butt
Max Planck Institute for Polymer Research
Ackermannweg 10, 55128 Mainz, Germany
E-mail: butt@mpip-mainz.mpg.de
Y. Wang
School of Mechanical Engineering
Southeast University
Nanjing 211189, China
K. Amann-Winkel
Institute for Physics
Johannes Gutenberg University Mainz
Staudingerweg 10, 55128 Mainz, Germany

The ORCID identification number(s) for the author(s) of this article can be found under https://doi.org/10.1002/adma.202311470

DOI: 10.1002/adma.202311470

$g = 9.81\ \mathrm{m\ s^{-2}}$) exceeds the capillary force F_0, which is the main component of the static friction force

$$F \approx F_0 = w\gamma k(\cos\Theta_R^0 - \cos\Theta_A^0) \quad (1)$$

Here, w is the width of the drop's contact area, γ is the surface tension of the liquid, and $k \approx 1$ is a geometrical drop shape factor, and Θ_A^0 and Θ_R^0 are the static advancing and receding contact angles. The difference between Θ_A^0 and Θ_R^0 determines the onset of sliding. Because of the capillary force in Equation (1) low roll-off angles of a tiny drop (<100 µL) imply low contact angles hysteresis $\Theta_A^0 - \Theta_R^0$.

Nanoscopic PDMS coatings often lead to particularly low contact angle hysteresis.[1,6] Grafting-to.[15] and grafting-from.[16] methods have been developed to coat surfaces such as glass, Si wafers or textured structures with nanometer thick layers of PDMS. Different preparations result in different architectures of the polymer layers.[1,6] In previous work, the onset of sliding was correlated with the reduced grafting density, $\Sigma = \sigma\pi R_g^2$.[17] Here, σ is the grafting density in $\mathrm{m^{-2}}$ and R_g is the radius of gyration of the polymer in a melt. Empirically, the layer thickness was found to help predict the static friction changing.[1,6] Gresham et al. found that the static friction is minimal at 2–5 nm layer thickness.[17] In order to achieve low friction, grafted chains should fully cover the substrate with a homogeneous brush.

In this study, we focused on dynamic friction. Dynamic friction $F(U)$ is the force required to move a drop at a given velocity U. In a steady state it is related to energy dissipation (that is the work done to move the drop per unit time P) by $P = F(U) \times U$. Only when a drop is moving, it can dissipate energy. As far as we know, neither dynamic friction forces $F(U)$ have been systematically measured on PDMS layers, nor the relevant energy dissipation processes have been identified. To analyze which processes, dissipate energy and cause friction, we needed to look at dynamic friction. The questions we addressed were: what is the ideal layer thickness and architecture to achieve the lowest drop friction? Is the layer thickness a sufficient descriptor of dynamic drop friction or does the architecture of the brush influence drop friction? What are the relevant dissipation processes in thin PDMS layers during drop movement?

To answer these questions, we investigated how coating thickness and architecture influence drop sliding. Three methods of coating surfaces with PDMS were applied (**Table 1**), including one grafting-from method and two grafting-to methods. Grafting-from leads to PDMS chains anchored at one end to the solid substrate.[1] In one grafting-to method, we allowed the PDMS chain with one functional chloride end to bind to the surface. Both methods led to polymer brushes. In the other grafting-to method, the PDMS chains were able to spontaneously bind to the substrate by immersion in the melt. The chains are thought to split, catalyzed by water at the interface, and react with silanol groups.[18] Based on neutron reflectivity experiments Gresham et al. proposed that short precursor PDMS chains react only once but that high molecular mass PDMS chains can react multiple times. To test the different PDMS coatings, we imaged water drops sliding down tilted surfaces and obtained the friction force by solving the equation of motion. Layer thicknesses were measured by atomic force microscopy, X-ray reflectivity (XRR), and ellipsometry. The layer mobility variation, which results in the friction difference, was also characterized by atomic force microscope (AFM) friction measurements and by using fluorescence correlation spectroscopy (FCS). In addition, the interfacial water structure and polymer structure was explored using sum-frequency generation (SFG).

Table 1. Notations and properties of the PDMS layers coated on Si wafer.

	M_w [a]	Θ_A^0 [b] [°]	Θ_R^0 [b] [°]	Method	Thickness [c] [nm]
GT1_1350	1350	102	95	Grafting-to[15a,c]	1.8
GF_10 s	1750	104	98	Grafting-from[16a]	1.5
GF_30 min	2800	105	101	Grafting-from	2.3
GT1_3500	3500	106	101	Grafting-to	4.0
GT1_6000	6000	108	106	Grafting-to	4.7
GT1_14000	14000	108	103	Grafting-to	5.9
GT1_18500	18500	110	108	Grafting-to	6.8
GT2_SCT	9500	108	106	Grafting-to[15d]	7.3
GT1_30000	30000	109	104	Grafting-to	8.4
GT1_117000	117000	107	76	Grafting-to	19.0

[a] The M_w of brushes from GF is described in Section S1 of the Supporting Information. They are estimated by the change of thickness and stretch length in AFM retract process. The molecular weight of GT method refers to the original silicone oil from which the layer was formed. In particular for GT samples, the chains linked to the surfaces will have a lower molecular weight since the chains cleave before binding. [b] Θ_A^0 and Θ_R^0 are the static advancing and receding contact angles measured by goniometer. [c] Thickness is the unweighted average value measured from three independent methods.

2. Experimental Section

2.1. Si Wafers as Substrates

To reduce the contribution of electrostatic interactions,[19] P-doped silicon wafers were used as substrates. Silicon wafers (orientation: ⟨1-0-0⟩, resistivity: 10^{-20} Ω cm, polished, SiMat Inc.) were cleaned by sonication in hexane and ethanol for 3 min. Subsequently, the wafers were treated with oxygen plasma (Femto low-pressure plasma system, Diener electronic GmbH, Germany) for 5 min at 200 W to enhance their reactivity and generate surface hydroxyl groups.

2.2. Fabrication of PDMS Layers by Grafting-to Using Methyl-Terminated PDMS

Wafers were immersed in 20 mL methyl-terminated liquid PDMS (Sigma-Aldrich), with different molecular weights (M_w = 1350, 3500, 6000, 14000, 18500, 30000, and 117000 g $\mathrm{mol^{-1}}$) in an oven at 150 °C for 24 h. To reduce the influence of free silicon oil or other adsorbed organic molecules, PDMS surfaces were carefully rinsed before use. The wafers were washed with toluene at least three times to remove free PDMS.[15a,c] Since the PDMS brushes are of nanoscopic thickness and oligomers were removed, no dependence of contact angles on measurable contact time were observed.[15a] The samples were named as GT1_M_w, e.g., GT1_1350 and GT1_117000.

2.3. Fabrication of PDMS Brushes Coatings by Grafting-from

A reactive solution was prepared by dissolving 1.4 mL of dichlorodimethylsilane (DCDMS, Sigma-Aldrich) in 40 mL of water-saturated toluene. The oxygen plasma treated silicon wafers were immersed in the reactive solution for either 10 s or 30 min to allow the DCDMS to polymerize starting from surface hydroxyl groups. Afterward, the samples were washed three times in toluene to remove any unreacted monomers. The samples were named GF_10s and GF_30 min. The molecular weight of these brushes was evaluated as described in Section S1 of the Supporting Information.

2.4. Fabrication of PDMS Layer by Grafting-to Using Chlorine Terminated PDMS

Silicon wafers were immersed in a polydimethylsiloxane-chlorine terminated (Sigma-Aldrich) liquid. Afterward, the wafers were placed in a sealed container inside an oven at 120 °C for 12 h. Finally, the samples were washed three times with toluene, creating sample GT2_SCT.

2.5. Wetting Properties Measurement by Goniometer

Static advancing and receding contact angles as well as the roll-off angles of water on the surface were measured by an OCA 35 goniometer (DataPhysics Instruments, Germany). Side view videos of sessile drops were recorded when changing the volume of a sessile water drop gradually (1.0 µL s^{-1}) between 10 and 20 µL using a Hamilton syringe. Static advancing and receding contact angles were determined by fitting an ellipse model to the contour images. Roll-off angles of the water drop on surfaces were characterized by goniometer with a 33 µL drop by titling the platform at a speed of 0.1° s^{-1}. Each data point is the average of at least three individual measurements on different areas of the surface.

2.6. Tilted Plate Experiments

To characterize dynamic wetting, tilted plate experiments were conducted as previously reported.[19] 33 µL drops of distilled water (<1 µS cm^{-1}, Gibco, Thermo Fisher Scientific) were deposited at the top of a tilted platform by a grounded syringe needle (1.5 mm outer diameter), which was connected to a peristaltic pump (MINIPULS 3, Gilson). Before every experiment, the surface was neutralized by an ionizing air blower for 5 min (Aerostat PC ionizing air blower, Simco-Ion). The drops detached from a height of ≈5 mm, which was similar to the drop size itself to avoid drop rebouncing. The drops were neutralized by a grounded copper wire immediately after they landed on the surface. They were imaged from the side with a frame rate of 1000 or 2000 per second over a slide length of typically 4.5 cm using a FASTCAM Mini UX100 (Photron) with a TitanTL telecentric lens (×0.268, Edmund Optics). The videos were analyzed by open drop-shape analysis programmed in MATLAB. The dynamic contact angles were determined by applying a polynomial fit to each frame of the images. In the end, the drop velocity U, dynamic contact angles at the front (advancing contact angle, Θ_A) and rear (receding contact angle, Θ_R), and the length of the drops were analyzed. All the measurements were done at 20 ± 1 °C and at 20–40% relative humidity.

2.7. AFM Thickness Measurement

The layer thickness, thickness distribution mapping, and chain length measurements were performed with cantilevers having a nominal resonance frequency of $f = 70$ kHz and a nominal spring constant of $k_z = 2$ N m^{-1} (Brucker OLTESPA). The humidity was between 25% and 35%. Spring constants were determined by the thermal tune method.[20] Samples were imaged using the JPK NanoWizard 4 AFM. The "Quantitative Imaging" (QI) mode was used to obtain force–distance curves at every point of the 128 × 128 pixels with a scanning area of 3 × 3 μm^2 at a set point force of 5 nN (time per pixel 20 ms).

To determine the PDMS film thickness and obtain information about the PDMS chain length, force–piezodisplacement curves, briefly called "force curves", were recorded. In the approach part of force curves, the difference in piezoposition of the point where the tip first touched the surface and was pulled onto the film and the point where attractive and repulsive sample forces balanced was calculated. At this point there is no net force acting on the tip. This distance is called jump-in distance $L_{\text{jump-in}}$. Accordingly, the "PDMS chain length" in the retracting cycle was estimated. The difference in piezodisplacement was calculated for the point where attractive and repulsive forces balance and the point where the tip snaps off the surface, i.e., detaches from the PDMS chains. It is called "jump off distance" $L_{\text{jump-off}}$. It is important to note that this value may be lower than the real chain length because the point where the tip attaches from the PDMS chain may not be the end of the chain. The jump-in and jump-off distances were calculated for each force curve of the scan area automatically using a custom Python script (https://github.com/PranavSudersan/afm_surface_tension/blob/main/AFM_Liquid_Analyzer.ipynb).

2.8. X-Ray Reflectivity

X-ray reflectivity measurements were applied to measure the thickness of the PDMS layers. X-rays impinged on the sample at grazing incidence angles and probe scattering angles slightly above total reflection. At the interfaces of a film (PDMS, substrate), the electron density changes. The reflected X-ray intensity was measured as a function of 2θ. Kissing-fringes appear due to interference of the reflected X-rays at the different interfaces, the period of the fringes is inversely proportional to the thickness of the film.[21] A Rigaku SmartLab Instrument with a rotating Cu-Anode was used, at an X-ray energy of 8.04 keV. The measured XRR data were analyzed using the software package (SmartLab Studio II).[22]

2.9. Ellipsometry Measurement

The thickness of PDMS layers was also measured by an ellipsometer (Nanofilm EP3, laser wavelength 658 nm, Laser 50 mW) using a 10× lens and by fitting, using a dispersion model.[23] The

angle of incidence was 50°. The fitting parameters for the silicon wafer (refractive index: 3.836) and PDMS (refractive index: 1.428) were kept constant. The native SiO_2 layer (refractive index: 1.457) on the Si wafer was measured as 1.6 ± 0.1 nm. The error reflects the variation within a series of measurements.

2.10. Characterization of PDMS Layers

The thickness of the PDMS layers was measured using three independent methods (**Figure 1a**; Section S2, Supporting Information): AFM force curves using the jump-in distance,[24] XRR,[21] and ellipsometry.[23] The layer was sorted according to average thickness from these measurements. The results from the three thickness measurements were in good agreement up to $L = 6$ nm. For thicker layers, the difference in results obtained with different methods increased. One possible reason for the different results could be a nonuniform thickness of layers. To further analyze the thickness distribution across the surface, the AFM QI mode was utilized to map the surface thickness distribution using force curves (Figure S2b, Supporting Information). Typically, the thickness at different locations on one sample varied by ≈2 nm.

2.11. AFM Friction Measurement

The measurement was performed with a JPK NanoWizard 4 in water. The cantilever spring constant k_z and the sensitivity S_z in the lateral direction were calibrated using a noncontact method reported by Mullin and Hobbs.[25] PPP-CONT-W (NANOSENSORS, width: 50 µm, length: 450 µm, nominal resonance frequency: 13 kHz) was used as sensors. Friction was measured inside a water drop in contact mode. The applied normal force was adjusted from 30 to 10 nN. The friction force was measured over a scan size of 10 µm at a tip velocity of 10 µm s^{-1} (scan rate: 1 Hz). All measurements were carried out at 24 °C, measured inside the acoustic housing of the AFM.

2.12. FCS Measurement

FCS experiments were performed on a commercial confocal microscope (LSM 880, Carl Zeiss, Jena, Germany) using a C-Apochromat 40x/1.2 W (Carl, Zeiss, Jena, Germany) water immersion objective. A HeNe laser (λ = 633 nm) fiber coupled to the LSM 880 was used for the excitation of the terrylene diimide (TDI) dyes. The emission light in the spectral range of 650–700 nm was detected using a spectral detection unit (Quasar, Carl Zeiss, Jena, Germany). A glass coverslip coated with a PDMS layer infiltrated with TDI molecules was mounted in an Attofluor stainless steel chamber (Thermo Fisher Scientific, Waltham, MA, USA). The TDI dye molecules were infiltrated into the PDMS layer by adding a hexane solution on top, followed by hexane evaporation and vacuum annealing at 70 °C overnight. The chamber was then filled with 1 mL MiliQ water so that the PDMS layer was completely covered by water. The confocal detection volume was placed over the PDMS layer and FCS autocorrelation curves were recorded for 150 s in repetitions of 30 s. The experiments were performed multiple times at 3–7 different lateral positions on the layer. The experimental autocorrelation curves were fitted with an analytical equation for a 2D Brownian motion.[26]

$$G(\tau) = 1 + \left[1 + \frac{f_T}{1-f_T} e^{-\tau/\tau_T}\right] \frac{1}{N} \sum_{i=1}^{m} \frac{f_i}{1+\frac{\tau}{\tau_{D,i}}} \quad (2)$$

here, f_T and τ_T are the fraction and the decay time of the triplet state, respectively, and N denotes the average number of fluorescent species in the observation volume. f_i is the fraction of the fluorescent species possessing the diffusion time $\tau_{D,i}$. The diffusion coefficient D_i of the ith species is related to their diffusion time through $D_i = r_0^2/4\tau_{D,i}$ where r_0 is the radial dimension of the confocal volume. The fits were done using the ZEN 3.0 software (Carl Zeiss, Jena, Germany).

2.13. Heterodyne-Detected Sum-Frequency Generation (HD-SFG) Measurements

The noncollinear HD-SFG setup was used, the details of which are described elsewhere.[27] In short, a Ti:Sapphire regenerative amplifier laser system (Spitfire Ace, Spectra-Physics, centered at 800 nm, ≈40 fs pulse duration, 5 mJ pulse energy, 1 kHz repetition rate) was employed in this setup. A part of the output was guided to a grating-cylindrical lens pulse shaper to produce a narrowband visible pulse (10 µJ pulse energy, FWHM = ≈10 cm^{-1}). The other part of the output was used to generate a broadband infrared (IR) pulse (3.5 µJ pulse energy, FWHM = 530 cm^{-1}) through an optical parametric amplifier (Light Conversion TOPAS-C) with a silver gallium disulfide (AgGaS2) crystal. The IR and visible beams were first focused into a 200 nm thick ZnO deposited on a 1 mm thick CaF_2 window to generate a local oscillator (LO) signal.[28] Subsequently, the IR, visible, and LO beams were refocused by using a pair of off-axis parabolic mirrors. These beams overlapped spatially and temporally at the sample position at the angles of incidence of 33°, 38°, and 37°, respectively. A fused silica glass plate with a 1.5 mm thickness was used for phase modulation of the LO signal. The SFG signal from the sample interfered with the SFG signal from the LO, generating the SFG interferogram, which was then dispersed in a spectrometer (Shamrock 303i, Andor Technology) and detected by an EMCCD camera (Newton, Andor Technology).

PDMS brushes were prepared on SiO_2 plates (25 mm diameter, 2 mm thick, PI-KEM Ltd.) using the same grafting-to method (GT1) for the HD-SFG measurement. HD-SFG spectra were measured in an N_2 atmosphere to avoid spectral distortion due to water vapor. The measurement was conducted in the ssp polarization combination, where ssp denotes s-polarized SFG, s-polarized visible, and p-polarized IR beams. To control the height of the samples, a height displacement sensor (CL-3000, Keyence) was used. The peak area of the C–H peaks was obtained by fitting the $\mathrm{Im}\chi^{(2)}$ spectra with Lorentz curves. The complex-valued spectra of second-order nonlinear susceptibility ($\chi^{(2)}$) of the SiO_2–PDMS brush/water interfaces were obtained via the Fourier analysis of the interferogram and normalization with that of the SiO_2–PDMS brush/gold interface. The interferogram of the SiO_2–PDMS brush/gold interface was collected immediately before the sample measurement to ensure a precise

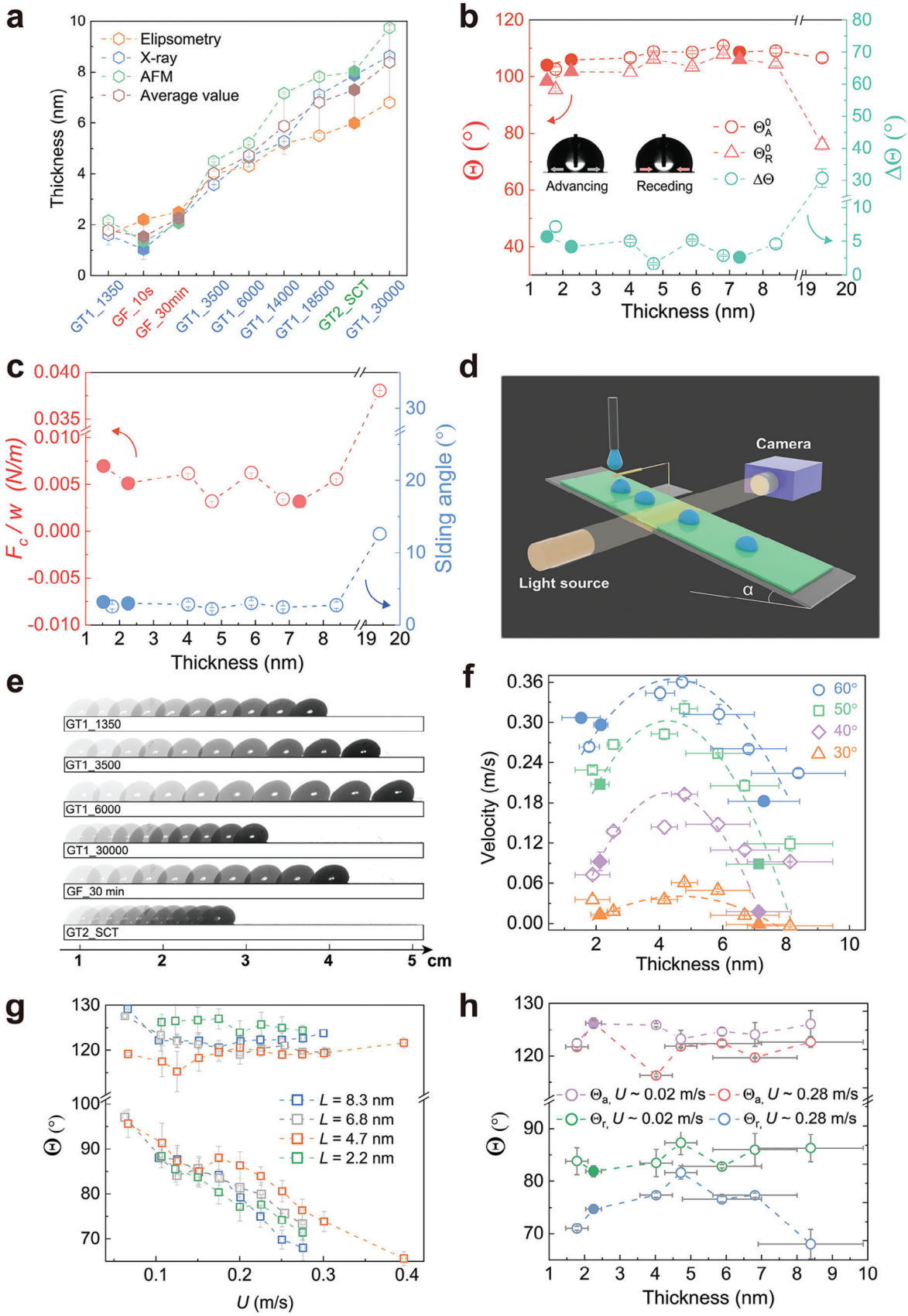

and stable reference phase. The phase of gold was determined based on the fact that the ($\mathrm{Im}\chi^{(2)}$) spectrum of the SiO_2–PDMS brush/D_2O interface shows a flat zero line. The error bars represent the 95% confidence interval of data measured on three different positions of the sample.

3. Results and Discussion

3.1. Static Wetting

To characterize the wetting properties of the PDMS layers (Figure 1a, Table 1), we measured the static advancing and receding contact angles of water on horizontal surfaces by gradually changing the drop volume at a rate of 1 µL s^{-1} in a goniometer. The static advancing Θ_A^0 and receding contact angles Θ_R^0 increased slightly up to a layer thickness of ≈4 nm (Table 1, Figure 1b). In parallel, the contact angle hysteresis, $\Delta\Theta = \Theta_A^0 - \Theta_R^0$, first decreased slightly from $\Delta\Theta \approx 7°$ ($L = 1.8$ nm thickness) to 5° ($L > 3$ nm). Then it remained constant and only at very high M_w (more than 100 kg mol^{-1}, $L = 19$ nm), did it increase again (Figure 1b). Here, we focus on results obtained by grafting-to, because they are directly comparable. Accordingly, the roll-off angles of 10 µL water drops were between 2° and 4° (Figure 1c) except for M_w = 117 kg mol^{-1}. The results agree with earlier reports,[1,15a,c,29] in which a minimum of contact angle hysteresis as a function of molecular weight or, correspondingly, viscosity of the PDMS is also observed. The precise positions and widths of the minimum varied substantially between the different reports, indicating that the properties of a PDMS layer depend on the specific conditions of preparation. The minimum is interpreted by the balance of two effects. At low thickness the surface is not yet perfectly covered by the PDMS. At high layer thickness the microviscosity of the PDMS layer is increased.

By means of the static advancing and receding contact angles, we can calculate the capillary force required for a drop to start sliding (Equation (1)). We call it "static friction force.".[14] To enable a comparison with other reports we plotted the static friction force divided by the width of the drop in Figure 1c. When inserting measured contact angles into Equation (1), the slight difference in contact angle hysteresis on different surfaces led to a shallow but not substantial minimum with respect to the layer thickness for $L < 10$ nm (Figure 1c, red points).

3.2. Drop Velocity and Dynamic Drop Friction Depends on the coating thickness

A constant roll-off angle indicates that the acceleration a drop undergoes in a tilted plate experiment is constant for different PDMS thicknesses. We expected that the velocity change of drops sliding down would also be identical (except for M_w = 117 kg mol^{-1}). However, the velocities of drops moving down tilted surfaces (Figure 1d) varied by up to a factor of 2 across the different PDMS-coated surfaces (Figure 1e). At 60° tilt and 4 cm slide distance, water drops reached a velocity of 0.36 m s^{-1} on GT1_6000. In contrast, on GT2_SCT it was only 0.18 m s^{-1} and on GT1_30 000 it was only 0.22 m s^{-1}. When plotting such drop velocity versus the PDMS layer thickness a peak velocity value was observed around a coating thickness of 5 nm (Figure 1f). This peak velocity at $L \approx 5$ nm was detected at a range of tilt angles (30° to 60°). We do not show results for lower titling angles because the drop velocity variation was too low. This thickness-dependent phenomenon was observed on PDMS-coated surfaces irrespective of the specific preparation. The surface roughness was indistinguishable for all layers prepared (Figure S3, Supporting Information). We conclude that the polymer layer thickness is the main predictive parameter for drop velocity. We further conclude that the dynamic friction force and thus energy dissipation depends on the PDMS layer thickness. Energy dissipation is minimal around a thickness of 5 nm.

To analyze the low energy dissipation at intermediate layer thickness, we measured dynamic advancing and receding contact angles (Θ_A and Θ_R) using the tilting platform at low and high drop velocities. Equation (1) can also be used to evaluate the dynamic drop friction per unit width,[14] provided the dynamic contact angles (Θ_A and Θ_R).[30] are inserted. To obtain dynamic contact angles over a wide range of velocities, experiments were carried out at tilt angles between 30° and 60°. The advancing contact angle remained constant with velocity for all the samples (≈120°). In contrast, the receding contact angles on different surfaces decreased with increasing drop velocity. They decreased by up to 20° ($L = 8.3$ nm) when the drop velocity reached more than 0.35 m s^{-1} (Figure 1g). For thin and thick PDMS layers, the receding contact angle decreased more with velocity than for a layer thickness ≈5 nm (Figure 1h). Thus, the reduced energy dissipation for 5 nm thick films is primarily situated at the receding contact line.

To further analyze dynamic drop friction, we estimated drop friction forces F in dynamic cases by evaluating the equation of motion as described before.[30]

$$F = mg\sin\alpha - m^*\frac{\mathrm{d}U}{\mathrm{d}t} \quad (3)$$

here, $m^* \approx 1.05m$ is an effective mass, which considers a rolling component of drop motion.[19] $m^*\frac{\mathrm{d}U}{\mathrm{d}t}$ represents the inertia of the drop. We extracted the drop position from the side view videos and calculated the velocity so that we could solve the equation of motion and obtain F versus U. This analysis is only an

Figure 1. Characterization of PDMS-coated surfaces and motion of water drops. a) Thickness values from three independent methods and average values corresponding to the different samples. b) The static advancing (Θ_A^0) and receding (Θ_R^0) contact angles and contact angle hysteresis $\Delta\Theta = \Theta_A^0 - \Theta_R^0$ versus the PDMS layer thickness. They were measured with a goniometer when both the advancing and receding contact line start to move. c) Capillary force per unit width calculated by Equation (1) for a 10 µL water drop. The drop width w was set to twice that of the drop contact radius.[19] d) The scheme of the tilted plate setup for drop velocity measurements and dynamic contact angles. e) Sequences of video side images of drops on different PDMS-coated surfaces. The time interval between images was 15 ms, the tilting angle was 60°, drop volume was 33 µL. f) Drop velocity versus PDMS layer thickness after 4 cm drop sliding at tilting angles of 60°, 50°, 40°, 30°. The dashed lines are to guide the eye. g) Dynamic advancing (Θ_A) and receding contact angles (Θ_R) versus drop velocity for different layer thicknesses. h) Dynamic advancing (Θ_A) and receding contact angles (Θ_R) measured by the titled plate versus layer thickness at a velocity of 0.02 and 0.28 m s^{-1}. All hollow symbols represent data from samples prepared by method GT1.

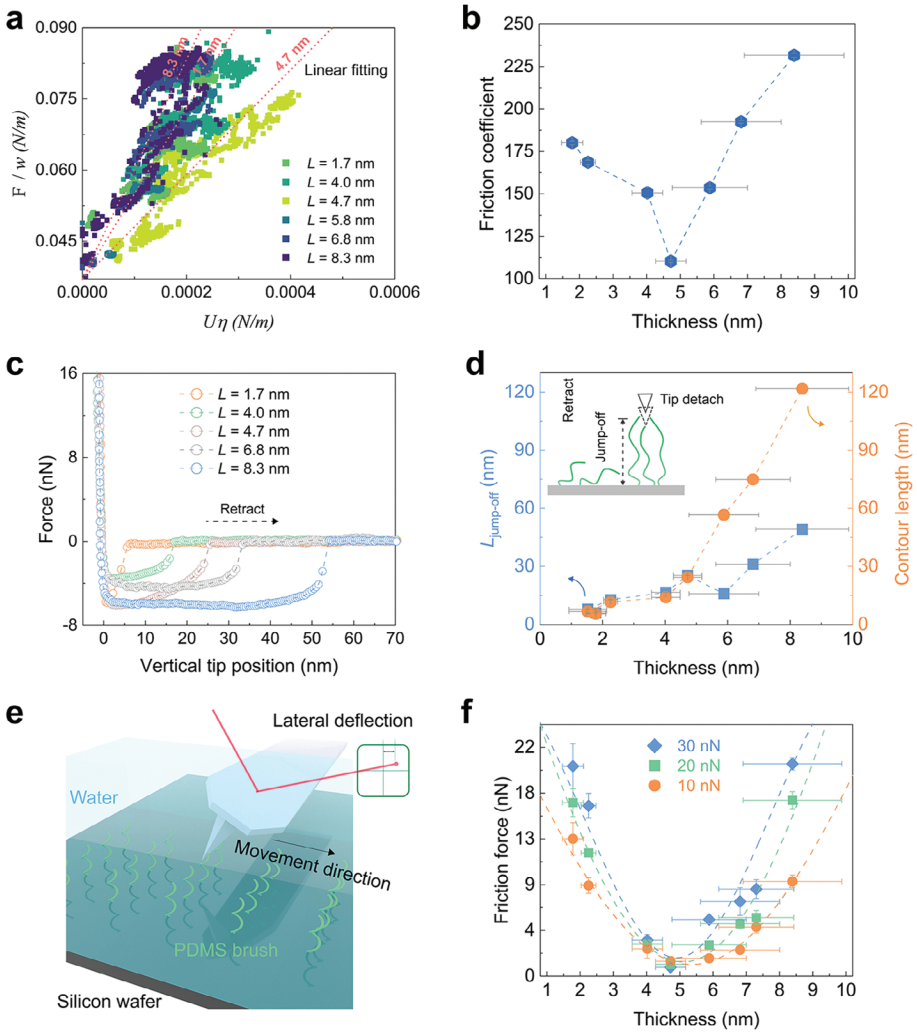

Figure 2. Friction of moving water drops. a) Linear fitting of the friction force (F) as a function of velocity. b) Friction coefficient (slope of the linear fitting) plotted versus the coating thickness. c) AFM retracting force curves obtained on various PDMS brush surfaces. d) "Jump-off distance" $L_{\text{jump-off}}$ and calculated contour lengths of the polymer chains versus layer thickness. e) The scheme to show the AFM measurement of the friction on PDMS brush surfaces in a water environment. f) Friction force versus the thickness measured at a load of 10, 20, and 30 nN (dashed lines are guides for the eye by Gaussian peak fitting).

approximate method because m^* depends slightly on velocity and we assumed that the drop is always in a steady state shape, without any vibrations.

When plotting drop friction versus velocity (**Figure 2a**), the force starts at a certain threshold given by Equation (1). Then it increased approximately linearly. The results can be fitted by.[30]

$$F = F_0 + \beta w \eta U \tag{4}$$

here, F_0 is a threshold force which needs to be exceeded to initiate drop motion (Equation (1)). β is a dimensionless friction coefficient. When plotting the F-versus-U slopes for various PDMS thickness, a minimum friction coefficient at 4.7 nm was observed (Figure 2a,b).

In our work, the grafting-to method from silicone oil (GT1) will most likely produce methyl end groups due to the reaction mechanism.[1,15d,18,31] For the other two methods, more terminal silanol groups will be produced due to the high activity of the chloride end.[32] Though the different end groups may affect drop friction,[31] the effect was not significant. We did not observe significantly different friction coefficients for PDMS layers prepared by the three different methods but with similar layer thickness.

3.3. Hypothesis to Explain the Minimum in Friction

What are the possible explanations for the observed minimum in the dependence of the friction on the PDMS layer thickness? While interpreting their data on $\Theta_A^0 - \Theta_R^0$ and static friction, Gresham et al.[17] concluded that "the PDMS chains must be sufficiently long and densely packed to uniformly coat the silicon wafers substrates, but not so tightly packed that chain entanglement compromises mobility." In the same way, we assume that

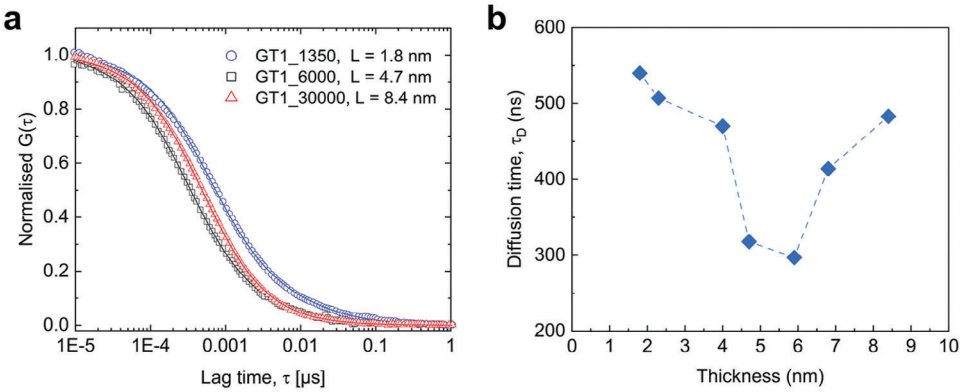

Figure 3. FCS measurements of tracer diffusion in PDMS layers. a) Typical autocorrelation curves and their corresponding fits for PDMS layer with low, medium, and high thickness. b) Diffusion time of TDI tracers versus PDMS layer thickness.

the thickness of the PDMS layer will significantly influence drop sliding and dynamic friction.

To test this hypothesis, we used FCS.[33] and monitored the diffusion of small tracer molecules in the PDMS layers. The mobility of tracer molecules is influenced by the heterogeneity and effective viscosity of the PDMS layer. In an FCS experiment, the fluctuations of fluorescent light intensity caused by the diffusion of fluorescent tracers through a small observation volume (<1 μm^3) were measured using a confocal microscope. A correlation analysis of these fluctuations provided information on the diffusion time τ_D that the tracers needed to cross the observation volume and similarly information on their diffusion coefficient and the mobility/viscosity of the environment.[33] Here, we studied the diffusion of small (≈1 nm) terylene diimide (TDI) dyes dispersed in a PDMS brush as described in the Experimental Section. For the FCS experiments the brushes were covered with water to better mimic the contact angle hysteresis and the drop sliding experiments. It should be noted, however, that no TDI molecules were observed in the water because they are hydrophobic and remained in the PDMS layer. Typical autocorrelation curves and their corresponding fits with Equation (2) are shown in **Figure 3**a. The diffusion times for all PDMS layers are plotted versus layer thickness in Figure 3b. The diffusion time τ_D shows a minimum for layers with intermediate thickness of ≈5 nm. TDI tracers diffused relatively quickly in such layers. Due to the high mobility of these PDMS layers the tracers experienced low local (nano) viscosity. For thicker layers the diffusion time increased, indicating lower mobility of the PDMS chains probably due to increased grafting density and entanglements. The diffusion time was highest and the mobility lowest in the very thin brushes.

As the autocorrelation curves measured on thin brushes could not be represented well with single component fits, a two-component model ($m = 2$ in Equation (2)) was used. The second component has only a small fraction (f_2 in Equation (2)) of 5–10% of the amplitude in the autocorrelation curve. The corresponding diffusion time, $\tau_{D,2}$ was several orders of magnitude slower than $\tau_{D,1}$. This extremely slow process is attributed to a temporal absorption of the TDI tracers to the glass substrate. Its presence indicates lower grafting density and inhomogeneities in the coating.

Inhomogeneity even down to the molecular scale increases drop friction, as recently reported for a series of octyltrichlorosilane-coated surfaces.[34] Inhomogeneity leads to local pinning of the contact line during drop sliding. Energy is dissipated as heat when at a specific point the stretched contact line depins and jumps back.

In addition, we propose that the effect of inhomogeneity may be enhanced by a destabilizing van der Waals disjoining pressure in the PDMS layer. Since the PDMS has the low T_g it can be considered as a liquid film. The van der Waals force exerted by the water on the top and the oxidized silicon wafer at the bottom causes a disjoining pressure across the film. The van der Waals force depends on the dielectric permittivity and the refractive indices of the media involved (water, PDMS, SiO_2, and Si). When using the permittivity and refractive index for amorphous SiO_2 ($\epsilon = 3.8$, $n = 1.457$), a weak, stabilizing disjoining van der Waals force is obtained (see the Supporting Information). We expect, however, that some water will penetrate the PDMS layer. The underlying SiO_2 is hydrated and may be even a gel-like layer. The equilibration between the water in the drop and the layer at the PDMS–SiO_2 interface is faster than 1 μs because PDMS takes up a few mM of water.[35] and the diffusion coefficient of water in PDMS is high.[35b,c] ($D \approx 2 \times 10^{-9}$ m^2 s^{-1}). Hydration of the interface will increase the dielectric permittivity and reduce the refractive index of the SiO_2 layer. Even a slight shift of ϵ and n will lead to a destabilizing van der Waals disjoining pressure at thin PDMS films (Figure S4, Supporting Information). Thus, van der Waals forces stabilize the PDMS layer at intermediate thickness while they may be weak or even destabilizing at low and high layer thickness because of the water penetration. Water interacts more strongly with the native oxide layer on the silicon wafer than with PDMS; this is one reason why the contact angle of water on Si wafers is lower than on PDMS. With increasing layer thickness, the distance between the surface of the Si wafer and water increases. As a result, the attraction between the Si wafer and water decreases. The initial increase in velocity can be attributed to the progressive thickening of the PDMS, thereby reducing the substrate effect. This reduced van der Waals force would also explain the increase in contact angles Θ_A and Θ_R for $L \lesssim 4$ nm.

Why does the friction coefficient increase for $L > 5$ nm (Figure 2b)? We argue that the effect is mainly caused by

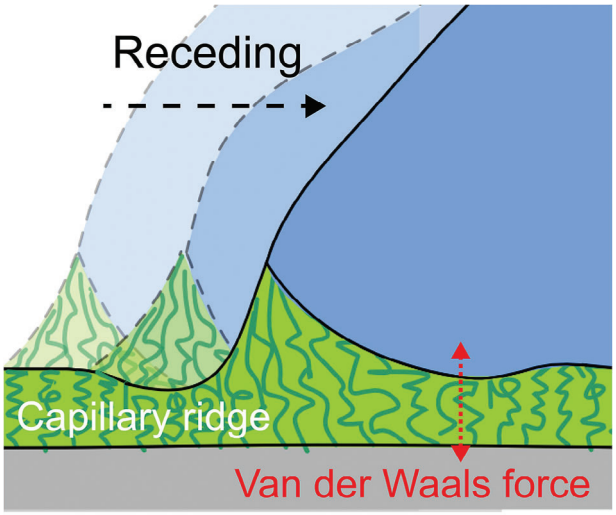

Figure 4. Schematic of the interaction between the PDMS brushes and a water drop near the moving contact line.

viscoelastic dissipation in the formation and shifting of a capillary ridge at the contact line.[11c] (**Figure 4**). The thicker the PDMS layer, the larger the PDMS capillary ridge caused by the polymer chain dragging, the more energy that is dissipated in drop motion. In prior research, it has been observed that energy dissipation of good solvent moving on PDMS brushes is caused by a possible elastic deformation at the contact line.[36] For poor solvent like water, energy is still dissipated because the PDMS chains in the capillary ridge are elastically stretched.[37] When they relax back to their initial configuration the energy is dissipated as heat. Therefore, viscous shear between the chains during the formation of the capillary ridge is directly dissipated. A third factor is the increase in interfacial areas (PDMS–air and water–PDMS), which may result in an interfacial energy change.

An important yet unsolved question concerns hydrodynamic viscous dissipation in the wedge of the water drop. On flat, infinitely rigid and homogeneous solid surfaces viscous dissipation due to flow of the liquid near the contact line is thought to be the dominating energy dissipation process at high velocity.[12a,38] Based on a flow field calculated by Huh and Scriven,[39] Kim et al. calculated the energy dissipation per unit contact line caused by wedge dissipation: $\Phi_w = 4c(\theta)\eta U^2 \ln(\Lambda/\lambda)$ with $c(\Theta) = \sin^2\Theta/2(\Theta - \sin\Theta\cos\Theta)$.[40] Here, Θ is the contact angle. Λ is a macroscopic length scale of typically 1 mm (size of the drop or capillary length) and λ is a cutoff length; below a length scale λ the usual no-slip boundary condition is relaxed. It is typically set to the order of 1 nm. Thus, viscous dissipation in the wedge critically depends on the boundary condition near the contact line. This boundary condition can change when the substrate is flexible enough. Elastic substrates react by deforming due to large local shear stress. A change of a factor of 10 in the cutoff length λ would change energy dissipation by a factor of 2.3.

3.4. AFM Experiments

To support the hypothesis of energy dissipation by nanoscopic ridge formation we further analyzed the retracting part of AFM force curves. The main question is: could the work done to form and move a nanoscopic capillary ridge of PDMS along the contact line account for the energy dissipation leading to dynamic drops friction? When retracting the AFM tip from the PDMS layer (Figure 2c), the attractive force (F_{att}) typically increased to F_{att} = 3–6 nN. Then it remained relatively constant up to a characteristic jump-off distance $L_{jump\text{-}off}$. The jump-off happened at a distance between 6 nm (GT1_1350) and 50 nm (GT1_30000). We compared the jump-off distance to the contour length of the polymer chains calculated from the maximum molecular weight. Up to $L \approx 5$ nm, the jump-off distance agreed with the calculated chain length (Figure 2d). For thicker layers, the measured jump-off distance was 2–3 times lower than the contour length. This lower jump-off distance for films formed from long chains is consistent with the hypothesis of Gresham et al., that long PDMS chains break multiple times into shorter chains.[17] The AFM retracting curves did not show any stretching of single chains, which would lead to an order of magnitude of lower forces.[41] We interpreted the attractive forces as the stretching of a PDMS meniscus formed by bundles of polymer chains. Since PDMS is nearly incompressible, it behaves like a molten film.

The formation of such a nanoscale capillary ridgeon a polymer brush has been simulated by Thiele and co-workers.[8d,42] To estimate, if ridge formation dissipates enough energy to substantially contribute to drop friction, we assume that the meniscus formed on a retracting AFM tip has similarities to the capillary ridge formed at a contact line. The difference is the radial symmetry for the AFM tip while the symmetry is along a line for the drop (**Figure 5**). We use this similarity to estimate the work carried out at the contact line from AFM measurements. The work required to form the meniscus with an AFM tip W_{att} can be estimated from the integral underneath the force-versus-distance curve (Figure 2d). It increased from $W_{att} \approx 4 \times 10^{-17}$ J for a 4 nm thick PDMS layer to 3×10^{-16} J for 8 nm thick layers. It is roughly given by $W_{att} \approx F_{att} L_{jump-off}$. To reach an attractive force of F_{att} by the surface tension of water one would need a contact line of length l given by $F_{att} = \gamma l \sin\theta$. θ is the contact angle of water on the brush. Here, for simplicity and because the contact angles are of the order of 90°, we set $\sin\theta = 1$. Thus, to reach an attractive force of 3–6 nN, the contact line of a water drop would need to be l = 42–83 nm long. The corresponding work done at the contact line per unit length would be $w_m = W_{att}/l$. Inserting W_{att} from above and with $l = \gamma/F_{att}$ we get $w_m = F_{att} L_{jump\text{-}off} / (F_{att}/\gamma) = L_{jump\text{-}off}\, \gamma$. This work per unit length due to the formation of a capillary ridge increased because $L_{jump\text{-}off}$ increases with the thickness of the PDMS layer (Figure 2f).

In a dynamic case, there is a continuous formation and release of capillary ridge at the front and rear contact lines. The question is if the energy dissipated by the formation of a capillary ridge is sufficiently high to account for drop friction. If we assume that the contact line forms a new ridge every slide distance Δx (rather than considering a continuous movement), the work carried out by the contact line would be $2F\Delta x/w$. Considering that the drop has a front and rear contact line we added a factor of 2. This work is equivalent to w_m. Thus, in case energy dissipation is only caused by forming and shifting the capillary ridge, the equivalent of one capillary ridge needs to be formed every lateral distance Δx estimated by $\Delta x = 2w_m w/F$.

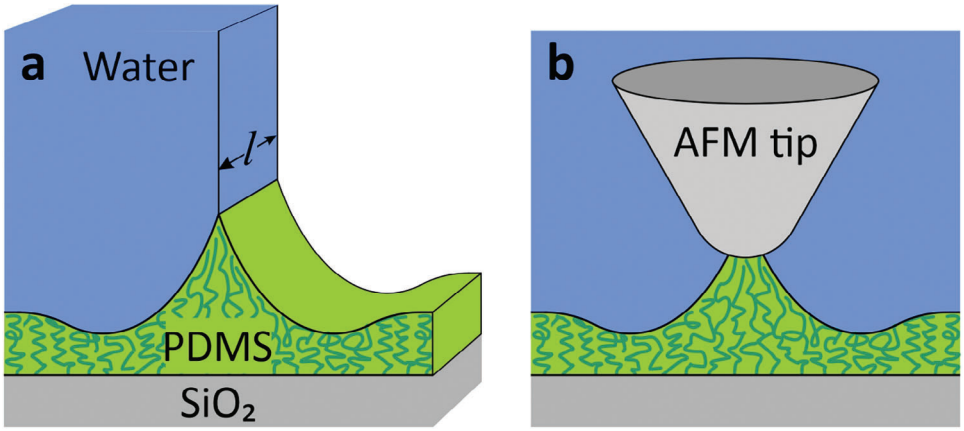

Figure 5. Schematic of a) the water static contact line and b) the AFM tip pulling on the PDMS brush.

The typical scaled friction force of a drop on PDMS surface was $F/w = 0.06$ N m^{-1} (Figure 2a). Inserting typical values, we obtain $\Delta x = 34$ nm for $L = 4$ nm thickness and 67 nm for 8.4 nm thickness. Since Δx cannot be larger than the contour length of the attached PDMS chains (≈30 nm for 8.4 nm thickness corresponding to jump-off distance in Figure 2d), we expect that viscoelastic energy dissipation at the three-phase contact line (Figure 4) by the drag process contributes substantially to drop friction at such a high thickness.

To support our view on energy dissipation, we measured friction forces using AFM tips (Figure 2e). Similar to the contact line of a moving drop, the tip will deform the PDMS layer locally. The PDMS will form a meniscus around the tip which will shift when the tip is moved laterally over the surface. The main difference is the different symmetry. Underneath a drop, the polymer layer is deformed along a line. In the AFM experiments, it is deformed around a central point. In addition, a load is applied by the AFM tip while the contact line of a drop only applies a tensional force. The AFM experiments were carried out underwater (Figure 2e). The applied loads ranged from 30 to 10 nN. Initially, the AFM tip was brought into contact with the PDMS surface at a load of 30 nN. Then friction force was measured by calibrating the lateral deflection of the cantilever tip over a 10 µm distance (Figure 2d; Figure S5, Supporting Information). Then the load was reduced to 20 and 10 nN, and the friction force was measured again (Figure 2f). At low layer thickness (<3 nm), the friction force was high. High friction illustrates more torsion when the tip slides on the coating. Then, a pronounced minimum in the friction force was observed for all applied loads, irrespective of the specific architecture of the layer. Once the thickness exceeded ≈ 6 nm, the friction increased again with thickness. If we divide the lowest AFM friction force by the equivalent length of a contact line of the order of 50 nm,[43] the friction force per unit length is ≈0.1 N m^{-1}, which agrees with the drop friction we measured in magnitude.

In addition to the effects proposed by Gresham et al.[17] and by our group, other factors may be of significance. Our understanding of drop friction is certainly not yet complete. One gap in knowledge is our poor understanding of interface architecture at a molecular scale. For this reason, we carried out additional experiments to learn more about how the structure of water at the PDMS–water interface related to drop friction.

3.5. SFG Spectroscopy

To understand the interfacial water organization and polymer organization at the polymer–water interface on different samples, we carried out the HD-SFG measurement at the interface of water and the PDMS layer supported by a SiO_2 substrate (**Figure 6a**; Figure S6, Supporting Information). The Im$\chi^{(2)}$ spectra (Figure 6b) show the broad O—H stretch of water features spanning from 2950 to 3550 cm^{-1} as well as the C—H stretch modes of the terminal —CH_3 group of the polymer (antisymmetric C–H stretch mode at 2940 cm^{-1} and symmetric C–H stretch mode at 2880 cm^{-1}).[44]

The O–H stretch Im$\chi^{(2)}$ bands are positive irrespective of PDMS layer thickness, indicating that the water dipole moment points up from the bulk water to the PDMS layer. To quantify the spectral area in the Im$\chi^{(2)}$ bands, we integrated the spectra from 3000 to 3500 cm^{-1} (Figure 6b; Figure S7, Supporting Information) only using the GT1 samples to prevent the effect from the terminated silanol groups in GF or GT2 (Figure S8, Supporting Information). The data are shown in Figure 6c revealing that the peak area is maximized at a thickness of 4.7 nm. The large (small) peak area of the O—H stretch mode indicates more (less) ordering of the interfacial water. Thus, the SFG data suggest that the interfacial water is the most ordered for the sample with a thickness of 4.7 nm (Figure 6b,c).

How can the water–polymer interface alter the SFG signal and drop friction? To answer this question, we first obtained the ratio of the symmetric stretch peak area versus the antisymmetric stretch peak area. The ratio of the symmetric/antisymmetric stretch peak area is an indicator of the structural alignment of the polymer at the interface;[45] a smaller (larger) ratio of the symmetric/antisymmetric peak area indicates that the terminal —CH_3 group is randomized (ordered). In the case of the polymer with a thickness of ≈5 nm, the ratio is minimal, manifesting that the terminal —CH_3 group of the PDMS is more ordered for the sample with its thickness of ≈5 nm (Figure 6b,c). When the PDMS layer thickness is smaller than

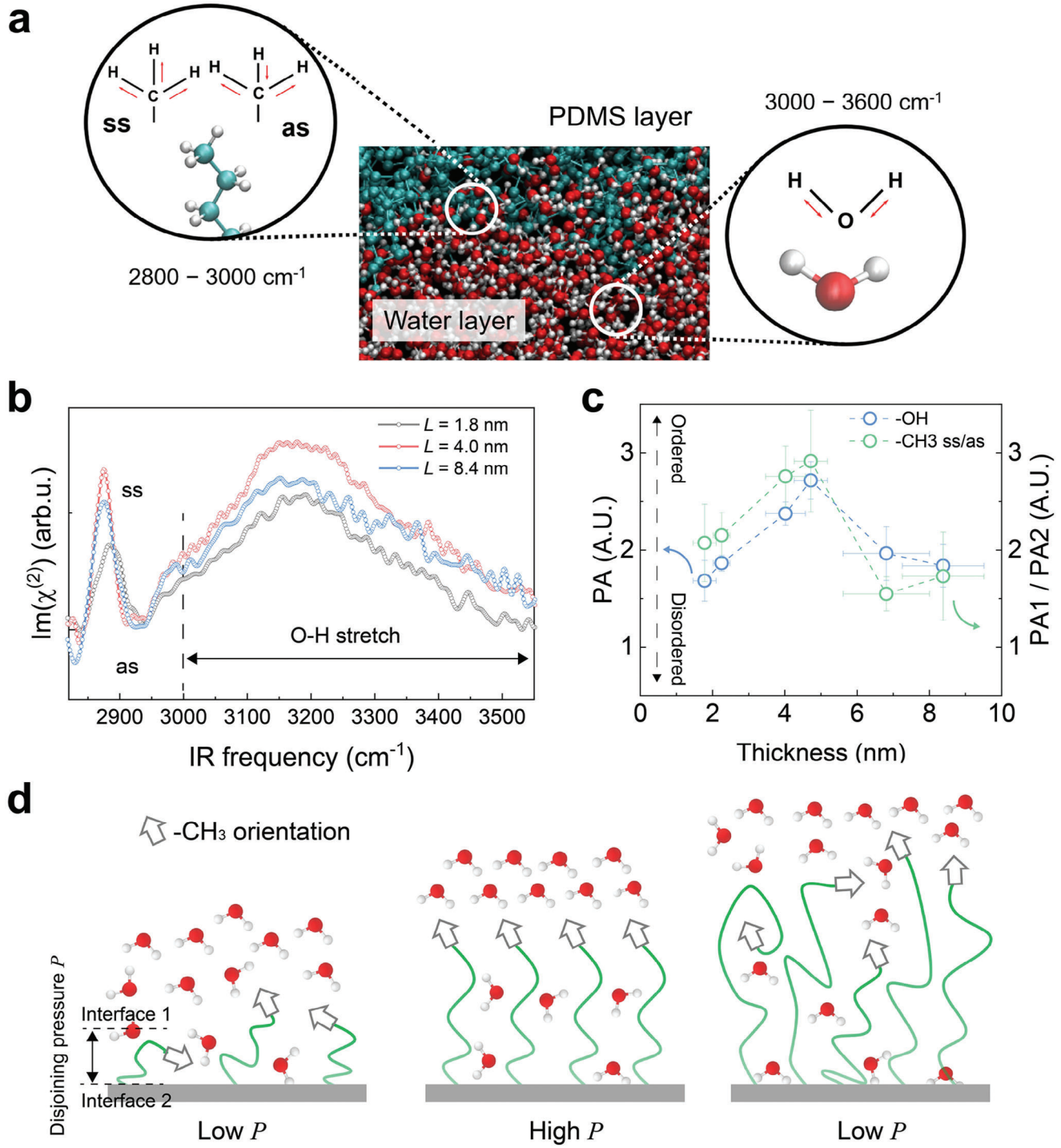

Figure 6. The impact of coating thickness variations on the interfacial water. a) Schematic of the PDMS/water interface. The red, green, and white spheres indicate oxygen, carbon, and hydrogen atoms, respectively. Atoms other than carbon atoms are removed from the PDMS layer for simplicity. The vibrational mode probed by the SFG spectroscopy is also illustrated. Symmetric stretch and antisymmetric stretch modes are denoted as "ss" and "as", respectively. b) SFG stretching spectra obtained at the SiO_2-supported PDMS/water interface for various PDMS brush surfaces. c) Changes in peak area of the O–H stretch mode $\mathrm{Im}\chi^{(2)}$ signatures (PA) spanning from 3000 to 3500 cm^{-1} in (b) versus thickness of the coating thickness and the ratio of symmetric (PA1) to antisymmetric (PA2) stretches peak area of C—H bonds in (b) versus the coating thickness. A higher value illustrates a more ordered water molecule and a more ordered polymer tail at the interface. d) Schematic representation of the ordered and disordered water and polymer tail at the interface detected by SFG with the thickness increasing.

≈5 nm, the surface is more randomized. The polymer chains are more or less self-organized. When the PDMS layer thickness is larger than ≈5 nm, the polymer chains are again more disordered, as the terminal of the polymer chains are too long to support their ordered structure. A sketch diagram of the interfacial water and polymer molecules organizations is shown in Figure 6d.

Such a behavior of the organization of the polymer is in line with the hypothesis of a strong stabilizing van der Waals force across the PDMS layer at intermediate thickness. For intermediate layer thickness, the polymer–water interface is stabilized by a disjoining pressure ≈10^4 Pa (Figure S4b, Supporting Information). In contrast, for $L > 5$ nm or below 2 nm, the ordering of the polymer interface and interfacial water is reduced because of the lower or even destabilizing van der Waals force per unit area (disjoining pressure).

4. Conclusions

In this work, we focus on the dynamic friction of water drops moving on a nanoscopic PDMS layer. The energy dissipation depends on the thickness L of the layers. The lowest dynamic friction is achieved at a brush thickness around 4.7 nm. We explain the increasing friction below $L < 4$ nm with a decreasing homogeneity of the surface. Inhomogeneities hinder the smooth motion of the contact line. Inhomogeneities may be enhanced at low PDMS layer thickness by destabilizing van Waals forces. At intermediate PDMS layer thickness, van der Waals forces stabilize the PDMS layer with a disjoining pressure above 10 kPa. Assuming that the amorphous SiO_2 layer is hydrated, a low or even destabilizing van der Waals disjoining pressure is obtained for low thickness.

Another energy dissipation process is the viscoelastic motion of the capillary ridge in the PDMS layer. The vertical component of the surface tension of water leads to the formation of a capillary ridge at the contact line. This ridge moves with the drop and energy is dissipated. AFM force measurement showed that this effect becomes stronger for thicker layers. We attribute the increasing friction for thick PDMS layers (>5 nm) to the motion of this capillary ridge. It may be enhanced by an increasing microviscosity of PDMS chains.

FCS shows maximum mobility of tracer molecules at intermediate layer thickness. For $L < 4$ or $L > 6$ the mobility decreases. SFG measurements showed a decrease in the ordering of the polymer interface and interfacial water when the thickness is smaller or larger than 5 nm. Both observations are consistent with a stabilizing van der Waals disjoining pressure across the PDMS layer at intermediate thickness. At high and low thickness, van der Waals forces are either weak or may even be destabilizing.

Supporting Information

Supporting Information is available from the Wiley Online Library or from the author.

Acknowledgements

This work received funding from the European Research Council (ERC) under the European Union's Horizon 2020 research and innovation program (Grant Agreement No. 883631, DYNAMO: X.Z. and H.-J.B.). X.Z. was sponsored by the China Scholarship Council (CSC). The authors acknowledge financial support by the German Research Society (DFG) via the Priority Programme 2171 Dynamic wetting of flexible, adaptive, and switchable surfaces (Grant No. BE 3286/6-1: X.L., R.B., and H.-J.B.). The authors would like to thank Stefan Weber and Doris Vollmer for fruitful discussions. The authors also would like to be thankful for the technique help from Diego Cortes.

Open access funding enabled and organized by Projekt DEAL.

Conflict of Interest

The authors declare no conflict of interest.

Author Contributions

X.Z. and H.-J.B. designed the experiment. X.Z., P.S., and R.B. conducted the AFM related measurement and analysis. X.Z., Y.W., and Y.N. conducted the SFG measurement and analysis. X.Z. and K.A. carried out the X-ray measurement and analysis. X.Z. and X.L. conducted the drop velocity measurement and analysis. X.Z. and D.C. perform the adhesion force measurement. K.K. performed the fluorescence correlation spectroscopy measurement and analysis. X.Z., Y.W., X.L., P.S., K.A., Y.N., R.B., and H.-J.B. wrote the paper. All authors have approved the final version of this manuscript.

Data Availability Statement

The data that support the findings of this study are available from the corresponding author upon reasonable request.

Keywords

drop friction, interfacial water, liquid-like coating, microfluid, wetting

Received: October 31, 2023
Revised: May 14, 2024
Published online: May 27, 2024

[1] I. J. Gresham, C. Neto, *Adv. Colloid Interface Sci.* **2023**, *315*, 102906.
[2] H. Barrio-Zhang, É. Ruiz-Gutiérrez, S. Armstrong, G. McHale, G. G. Wells, R. Ledesma-Aguilar, *Langmuir* **2020**, *36*, 15094.
[3] a) H. Zhang, M. Chiao, *J. Med. Biol. Eng.* **2015**, *35*, 143; b) K. Golovin, A. Dhyani, M. D. Thouless, A. Tuteja, *Science* **2019**, *364*, 371.
[4] S. T. Milner, T. A. Witten, M. E. Cates, *Macromolecules* **1988**, *21*, 2610.
[5] a) B. Zhao, W. J. Brittain, *Prog. Polym. Sci.* **2000**, *25*, 677; b) D. Daniel, J. V. I. Timonen, R. Li, S. J. Velling, M. J. Kreder, A. Tetreault, J. Aizenberg, *Phys. Rev. Lett.* **2018**, *120*, 244503.
[6] L. Chen, S. Huang, R. H. A. Ras, X. Tian, *Nat. Rev. Chem.* **2023**, *7*, 123.
[7] a) B. Andreotti, J. H. Snoeijer, *Annu. Rev. Fluid Mech.* **2020**, *52*, 285; b) P. G. de Gennes, *Rev. Mod. Phys.* **1985**, *57*, 827.
[8] a) F. Léonforte, M. Müller, *J. Chem. Phys.* **2011**, 135; b) L. I. S. Mensink, J. H. Snoeijer, S. de Beer, *Macromolecules* **2019**, *52*, 2015; c) R. G. M. Badr, L. Hauer, D. Vollmer, F. Schmid, *J. Phys. Chem. B* **2022**, *126*, 7047; d) S. Hartmann, J. Diekmann, D. Greve, U. Thiele, *Langmuir* **2024**, *40*, 4001.
[9] a) R. W. Style, A. Jagota, C.-Y. Hui, E. R. Dufresne, *Annu. Rev. Condens. Matter Phys.* **2017**, *8*, 99; b) R. W. Style, R. Boltyanskiy, Y. Che, J. S. Wettlaufer, L. A. Wilen, E. R. Dufresne, *Phys. Rev. Lett.* **2013**, *110*, 066103; c) E. R. Jerison, Y. Xu, L. A. Wilen, E. R. Dufresne, *Phys. Rev. Lett.* **2011**, *106*, 186103.

[10] S. J. Park, B. M. Weon, J. S. Lee, J. Lee, J. Kim, J. H. Je, *Nat. Commun.* **2014**, *5*, 4369.
[11] a) A. Carré, J.-C. Gastel, M. E. R. Shanahan, *Nature* **1996**, *379*, 432; b) M. Zhao, J. Dervaux, T. Narita, F. Lequeux, L. Limat, M. Roché, *Proc. Natl. Acad. Sci. USA* **2018**, *115*, 1748; c) H. K. Khattak, S. Karpitschka, J. H. Snoeijer, K. Dalnoki-Veress, *Nat. Commun.* **2022**, *13*, 4436.
[12] a) D. Bonn, J. Eggers, J. Indekeu, J. Meunier, E. Rolley, *Rev. Mod. Phys.* **2009**, *81*, 739; b) H. Song, D. L. Chen, R. F. Ismagilov, *Angew. Chem., Int. Ed.* **2006**, *45*, 7336.
[13] a) F. Chen, Y. Wang, Y. Tian, D. Zhang, J. Song, C. R. Crick, C. J. Carmalt, I. P. Parkin, Y. Lu, *Chem. Soc. Rev.* **2022**, *51*, 8476; b) E. Y. Bormashenko, *Wetting of Real Surfaces*, De Gruyter, Berlin **2019**; c) F. B.-W. P-G Gennes, D. Quéré, *Capillarity and Wetting Phenomena: Drops, Bubbles, Pearls, Waves*, Springer, New York, NY **2004**.
[14] N. Gao, F. Geyer, D. W. Pilat, S. Wooh, D. Vollmer, H.-J. Butt, R. Berger, *Nat. Phys.* **2018**, *14*, 191.
[15] a) H. Teisala, P. Baumli, S. A. L. Weber, D. Vollmer, H.-J. Butt, *Langmuir* **2020**, *36*, 4416; b) N. Singh, H. Kakiuchida, T. Sato, R. Hönes, M. Yagihashi, C. Urata, A. Hozumi, *Langmuir* **2018**, *34*, 11405; c) J. W. Krumpfer, T. J. McCarthy, *Langmuir* **2011**, *27*, 11514; d) K. Fazle Rabbi, J. Y. Ho, X. Yan, J. Ma, M. J. Hoque, S. Sett, N. Miljkovic, *Adv. Funct. Mater.* **2022**, *32*, 2112837; e) A. Viallat, J. P. Cohen-Addad, A. Pouchelon, *Polymer* **1986**, *27*, 843; f) N. Celik, S. Akay, F. Sahin, G. Sezer, E. Dagasan Bulucu, M. Ruzi, H.-J. Butt, M. S. Onses, *Adv. Mater. Interfaces* **2023**, *10*, 2300069.
[16] a) J. Liu, Y. Sun, X. Zhou, X. Li, M. Kappl, W. Steffen, H.-J. Butt, *Adv. Mater.* **2021**, *33*, 2100237; b) L. Wang, T. J. McCarthy, *Angew. Chem., Int. Ed.* **2016**, *55*, 244.
[17] I. Gresham, S. Lilley, A. Nelson, K. Koynov, C. Neto, *Angew. Chem., Int. Ed.* **2023**, *62*, 202308008.
[18] G. Graffius, F. Bernardoni, A. Y. Fadeev, *Langmuir* **2014**, *30*, 14797.
[19] X. Li, P. Bista, A. Z. Stetten, H. Bonart, M. T. Schür, S. Hardt, F. Bodziony, H. Marschall, A. Saal, X. Deng, R. Berger, S. A. L. Weber, H.-J. Butt, *Nat. Phys.* **2022**, *18*, 713.
[20] I. A. Soldatenkov, *Wear* **2008**, *29*, 7.
[21] M. F. Toney, C. M. Mate, K. A. Leach, D. Pocker, *J. Colloid Interface Sci.* **2000**, *225*, 219.
[22] M. Yasaka, *The Rigaku Journal* **2010**, *26*, 1.
[23] J. Sancho-Parramon, M. Modreanu, S. Bosch, M. Stchakovsky, *Thin Solid Films* **2008**, *516*, 7990.
[24] S. Li, Y. Hou, M. Kappl, W. Steffen, J. Liu, H.-J. Butt, *Adv. Mater.* **2022**, *34*, 2203242.
[25] N. Mullin, J. K. Hobbs, *Rev. Sci. Instrum.* **2014**, *85*, 113703.
[26] N. Kahya, P. Schwille, *Mol. Membr. Biol.* **2006**, *23*, 29.
[27] Y. Wang, T. Seki, X. Liu, X. Yu, C.-C. Yu, K. F. Domke, J. Hunger, M. T. M. Koper, Y. Chen, Y. Nagata, M. Bonn, *Angew. Chem., Int. Ed.* **2023**, *62*, 202216604.
[28] H. Vanselous, P. B. Petersen, *J. Phys. Chem. C* **2016**, *120*, 8175.
[29] a) D. H. Flagg, T. J. McCarthy, *Langmuir* **2017**, *33*, 8129; b) J. Sarma, L. Zhang, Z. Guo, X. Dai, *Chem. Eng. Sci.* **2022**, *431*, 133475.
[30] X. Li, F. Bodziony, M. Yin, H. Marschall, R. Berger, H.-J. Butt, *Nat. Commun.* **2023**, *14*, 4571.
[31] B. Khatir, Z. Azimi Dijvejin, P. Serles, T. Filleter, K. Golovin, *Small* **2023**, *19*, 2301142.
[32] S. F. Thames, K. G. Panjnani, *J. Inorg. Organomet. Polym.* **1996**, *6*, 59.
[33] K. Koynov, H.-J. Butt, *Curr. Opin. Colloid Interface Sci.* **2012**, *17*, 377.
[34] a) S. Lepikko, Y. M. Jaques, M. Junaid, M. Backholm, J. Lahtinen, J. Julin, V. Jokinen, T. Sajavaara, M. Sammalkorpi, A. S. Foster, R. H. A. Ras, *Nat. Chem.* **2024**, *16*, 506; b) S. M. Flores, A. Shaporenko, C. Vavilala, H.-J. Butt, M. Schmittel, M. Zharnikov, R. Berger, *Surf. Sci.* **2006**, *600*, 2847.
[35] a) J. A. Barrie, D. Machin, *J. Macromol. Sci., Part B: Phys.* **1969**, *3*, 645; b) J. M. Watson, M. G. Baron, *J. Membr. Sci.* **1996**, *110*, 47; c) S. J. Harley, E. A. Glascoe, R. S. Maxwell, *J. Phys. Chem. B* **2012**, *116*, 14183.
[36] a) R. Lhermerout, K. Davitt, *Colloids Surf., A* **2019**, *566*, 148; b) R. Lhermerout, H. Perrin, E. Rolley, B. Andreotti, K. Davitt, *Nat. Commun.* **2016**, *7*, 12545.
[37] D. Long, A. Ajdari, L. Leibler, *Langmuir* **1996**, *12*, 1675.
[38] J. H. Snoeijer, B. Andreotti, *Annu. Rev. Fluid Mech.* **2013**, *45*, 269.
[39] C. Huh, L. E. Scriven, *J. Colloid Interface Sci.* **1971**, *35*, 85.
[40] H.-Y. Kim, H. J. Lee, B. H. Kang, *J. Colloid Interface Sci.* **2002**, *247*, 372.
[41] S. Al-Maawali, J. E. Bemis, B. B. Akhremitchev, R. Leecharoen, B. G. Janesko, G. C. Walker, *J. Phys. Chem. B* **2001**, *105*, 3965.
[42] D. Greve, S. Hartmann, U. Thiele, *Soft Matter* **2023**, *19*, 4041.
[43] J. Eggers, H. A. Stone, *J. Fluid Mech.* **2004**, *505*, 309.
[44] a) I. V. Stiopkin, H. D. Jayathilake, A. N. Bordenyuk, A. V. Benderskii, *J. Am. Chem. Soc.* **2008**, *130*, 2271; b) L. Wang, T. Ishiyama, A. Morita, *J. Phys. Chem. A* **2017**, *121*, 6701.
[45] N. Takeshita, M. Okuno, T.-A. Ishibashi, *Phys. Chem. Chem. Phys.* **2017**, *19*, 2060.